第36卷第3期
2017年6月

红外与毫米波学报
J. Infrared Millim. Waves

Vol. 36, No. 3
June, 2017

文章编号: 1001-9014(2017)03-0280-04

DOI: 10.11972/j.issn.1001-9014.2017.03.006

Watt-class low divergence 2 μm GaSb based broad-area quantum well lasers

XING En-Bo[1,2], RONG Jia-Min[1,2], ZHANG Yu[3], TONG Cun-Zhu[1,*], TIAN Si-Cong[1], WANG Li-Jie[1], SHU Shi-Li[1], LU Ze-Feng[1,2], NIU Zhi-Chuan[3], WANG Li-Jun[1]

(1. State Key Laboratory of Luminescence and Applications, Changchun Institute of Optics, Fine Mechanics and Physics, Chinese Academy of Sciences, Changchun 130033, China;
2. University of Chinese Academy of Sciences, Beijing 100049, China;
3. Institute of Semiconductors, Chinese Academy of Sciences, Beijing 100083, China)

Abstract: GaSb based broad-area (BA) diode lasers with watt-class emission power and improved divergence were demonstrated using a fishbone shape microstructure. The influences of etching depth of microstructure on the emission and far-field performance were investigated. It was found that the utilization of microstructure was able to enhance the emission power evidently. Moreover, the deeply etched microstructure was more effective on the decrease of mode number and lateral far-field divergence. Compared with the device without microstructure, the deeply etched BA lasers show 57% decrease in the lateral far-field angle defined by the 95% power content, and the maximum continuous-wave (CW) output power exceeds 1.1 W.

Key words: GaSb based, broad-area (BA) diode lasers, microstructure, lateral far-field divergence
PACS: 42.55.Px, 42.60.Jf, 42.62.Fi

2微米波段低发散角瓦级GaSb基宽区量子阱激光器

邢恩博[1,2], 戎佳敏[1,2], 张 宇[3], 佟存柱[1,*], 田思聪[1], 汪丽杰[1], 舒适立[1], 卢泽丰[1,2], 牛智川[3], 王立军[1]

(1. 中国科学院长春光学精密机械与物理研究所, 吉林 长春 130033;
2. 中国科学院大学, 北京 100049;
3. 中国科学院半导体研究所, 北京 100083)

摘要: 通过在宽区GaSb基半导体激光器波导中引入鱼骨型微结构, 实现了瓦级激光输出并且改善了侧向发散角. 本文通过分析微结构的刻蚀深度对激光功率和远场特性的影响, 研究并发现了微结构的引入可以明显的提高激光器输出功率, 同时深刻蚀的微结构对降低模式数和侧向发散角有着更明显的改善作用. 相比于未引入微结构的激光器, 引入深刻蚀微结构的宽区激光器侧向95%功率定义的远场发散角降低了大约57%, 并且实现了超过1.1 W的最大连续输出功率.

关 键 词: *GaSb*基; 宽区激光器; 微结构; 远场发散角

中图分类号: TN248.4 **文献标识码:** *A*

Introduction

High power mid-infrared GaSb based lasers are desired for many applications, such as gas sensing, liquid sensing, light detection and ranging (LiDAR), laser spectroscopy and medical applications [1-6]. For high power emission, the broad-area (BA) structure is the prima-

Received date: 2016-08-31, **revised date:** 2017-02-17 **收稿日期:** 2016-08-31, **修回日期:** 2017-02-17
Foundation items: Supported by National Natural Science Foundation of China (61404138, 61474119, 61435012), the National Basic Research Program of China (2013CB64390303), Jilin Provincial Natural Science Foundation (20160101243JC and 20150520105JH), and the International Science Technology Cooperation Program of China (2013DFR00730)
Biography: Xing En-Bo (1986-), male, Jilin China, Ph. D. candidate. Research field is Photonic crystal lasers and Semiconductor lasers. E-mail: xiaoxing1228@126.com
* **Corresponding author:** E-mail: tongcz@ciomp.ac.cn

ry choice and has been widely studied [7-9]. However, a recognized drawback for BA diode lasers is the high lateral divergence due to the allowance of multiple lateral modes operation, so the expensive optical elements with high numerical aperture (NA) will be required for these devices for focusing and coupling purposes. Hence, the suppressing of lateral modes in BA lasers is crucial for the realization of high power and high beam quality GaSb based diode lasers. Some approaches for controlling the lateral modes have been proposed and investigated, such as the external cavities [10-11], curved waveguide [12], anti-guiding layer [13], leaky ridge-waveguide [14], tapered gain regions [15], microstructures [16-17] and Bragg gratings [18-19]. In our recent work, a fishbone microstructure was proposed and implemented in BA waveguide. The results show that the threshold current and output power can be improved [17].

In this letter, to achieve higher power and lower lateral divergence, we optimized the epitaxial structure and studied the characteristics of devices with different etching depth of microstructure. The light-injected current-voltage (L-I-V) characteristics, lateral far-field (FF) performance and lasing spectra were measured and analyzed.

1 Device fabrication

As the maximum output power of lasers in our recent work is just about 330 mW at 1.5 A [17], we optimized the epitaxial structure of GaSb based quantum well (QW) lasers. The device was designed with a typical total interface reflection (TIR) structure. To reduce the operation voltage and improve the output power, the aluminum concentration in the AlGaAsSb waveguide layers and cladding layers were respectively reduced from 0.35 and 0.6 to 0.2 and 0.5 compared with our recent work [17]. The epitaxial structure was grown on (100)-oriented 2-inch GaSb substrate by a solid-source VEECO Gen II molecular beam epitaxy (MBE) system. The active region was 10 nm $In_{0.2}Ga_{0.8}Sb$ QWs sandwiched between the symmetrical top and bottom 270 nm thick $Al_{0.2}Ga_{0.8}As_{0.02}Sb_{0.98}$ waveguide layers. The top and bottom cladding layers were respectively 2 μm thick p-doped and n-doped $Al_{0.50}Ga_{0.50}As_{0.02}Sb_{0.98}$, and the corresponding dopants were Be and Te, respectively. In addition, a 300 nm thick p+ GaSb layer was grown on the top of cladding layer for Ohm contact.

After the epitaxial growth, the standard fabrication processing was performed. The stripe mesa with width of 100 μm and depth of 2.3 μm was fabricated using standard contact optical lithography. The detail of fishbone microstructure is shown in Fig. 1, which consists of two row symmetrical trenches with linearly increased lengths from 5 μm to 35 μm by 5 μm step, and the width of single trench is 4 μm with a period of 9 μm. The microstructure was designed according to the distribution of lateral modes, more details can be found in Ref. [17]. To investigate the influence of etching depth of microstructure, the shallow depths of 1.6 μm and deep depth of 2.3 μm were formed by ICP. The electrical insulation layer of 200 nm Si_3N_4 was deposited by PECVD at

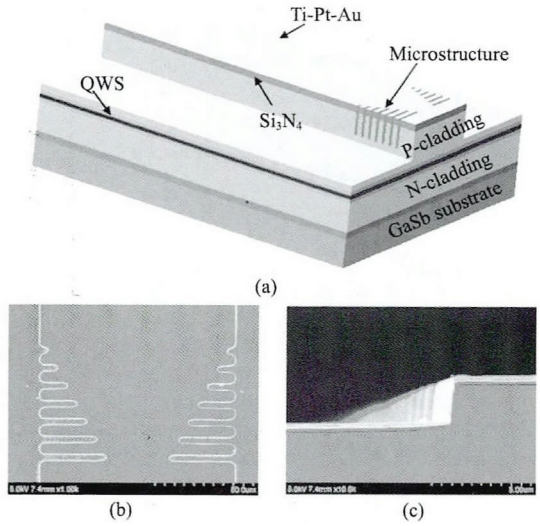

Fig. 1 (a) Schematic diagram of GaSb based BA lasers with the fishbone microstructure. (b) Scanning electron microscope photograph of the microstructure. (c) Scanning electron microscope photograph of the deep etching device on the vertical cross-section

图 1 (a) 引入微结构的 GaSb 基宽区波导激光器示意图. (b) 微结构的 SEM 图. (c) 深刻蚀垂直剖面 SEM 图

300℃. The contact window was 90 μm, whose opening was performed by reactive ion etching (RIE) using CF_4/O_2 gas. Then the p-type contact metal of Ti-Pt-Au and n-type metal of Au-Ge-Ni-Au were deposited. For accurate comparison, the devices without (W/O), with shallow (WSM) and with deep (WDM) fishbone microstructure were fabricated with the same cavity length of 1.4 mm. These laser devices were soldered by p-side down on the copper heat-sink without facet passivation and coating for testing.

2 Results and discussion

2.1 L-I-V characteristics

Figure 2 plots the measured light-current-voltage (L-I-V) curves of the InGaSb/AlGaAsSb QW BA lasers without, with shallow (1.6 μm) and deep (2.3 μm) microstructure at room temperature. The devices operated under continuous wave (CW) mode and were tested by Thorlabs PM1000 power meter with S401C pyroelectric energy sensor. As shown in Fig. 2, the maximum output powers of these samples are limited by the thermal roll-over. The voltage performances of W/O, WSM and WDM devices are almost the same, but it is worthy to note that the WSM and WDM devices show evident distinctions in the output power. The maximum powers (both facets) are respectively 0.91 W for W/O device, 1.113 W for WSM and 1.168 W for WDM devices. In the other word, the maximum output power of WDM device shows an increase of 28.5% compared with W/O devices. For the devices with microstructure, the increased output power might be attributed to the suppressing of high-order lateral modes [20-21], which lead to a more uniform near-field and better matching between the

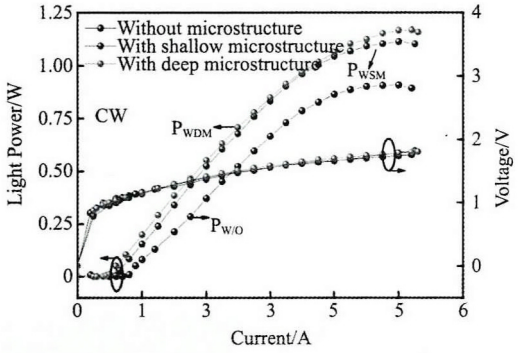

Fig. 2 L-I-V characteristics of GaSb-based BA lasers without (black symbol) , with shallow (blue symbol) and deep (purple symbol) microstructure at room temperature

图2 无结构,浅刻蚀微结构和深刻蚀微结构的宽脊型 GaSb 基激光器的 L-I-V 特性

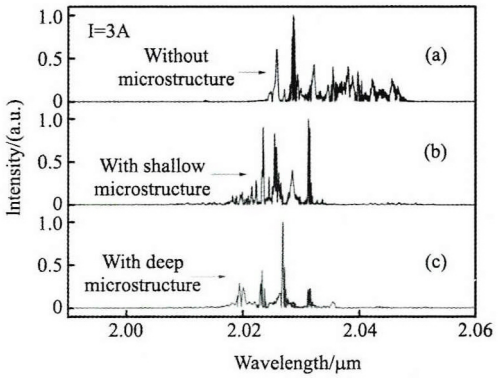

Fig. 3 Measured emission spectra of GaSb based BA lasers without (purple line) , with shallow (blue line) and with deep (red line) microstructure at 3 A

图3 电流为 3 A 时,无结构,浅刻蚀微结构和深刻蚀微结构的宽脊型 GaSb 基激光器的光谱特性

modal profile and injected current profile [20] . The deeply etched microstructure was closer to the upper waveguide than that in the WSM devices, so the high-order modes suffer from more losses and are also suppressed more evidently. The corresponding threshold currents are 0.9 A for W/O device, 0.7 A for WSM and 0.65 A for WDM devices, so the threshold current is also prominently decreased by the introduced microstructure. Moreover, the slope efficiencies are also improved correspondingly, which are increased to 0.226 W/A (WSM) and 0.233 W/A (WDM) , by contrast it is about 0.182 W/A for the W/O device.

2.2 Spectrum property

The lasing spectra of these three types of devices were measured by Bruker Vertex 70 FTIR spectrometer and shown in Fig. 3. Obviously, for the devices with microstructure (WSM and WDM) , it shows that the mode number from the spectra is significantly reduced compared with the W/O device. For the devices without microstructure, the measured spectrum is composed of many peaks with a span up to 28 nm, and the peak wavelength is 2.028 6 μm at 3 A, and for the devices with shallow and deep microstructures, the spans of spectra are less than 20 nm. These characteristics are agreed with the Ref. [17] . Moreover, for the devices with microstructure, the blue-shift of wavelength means that this structure can improve the heat dissipation. Compared with WSM devices, the spectra of WDM devices has less peaks and the side-modes with lower intensity. Therefore, the deep microstructure presents stronger compressing on the high-order lateral modes and hence less peaks in lasing spectra.

2.3 Far-field characteristics

As the microstructure only affects the mode distribution in lateral direction, the lateral FF profiles of W/O, WSM and WDM devices at different current were measured and shown in Fig. 4. The FF angle defined by full-width at half-maximum (FWHM) is not reasonable here due to the non-Gaussian distribution of lateral FF profiles. So in here the lateral FF angles defined by 95% power content will be more meaningful than FWHM for the description of FF angle in practical applications [22-23] . As shown in Fig. 4, the lateral FF angles defined by 95% power content for W/O (a) , WSM (b) and WDM (c) devices at 3 A were tested and analyzed. The lateral FF angle for the device with deep trenches ($\theta_{95\%,WDM}$) is only 17.5°, about 1.6° lower than that with shallow trenches. In Fig. 4(d) , as the injection current increases from 1 A to 3 A, the $\theta_{95\%,WDM}$ gradually increases from 14.9° to 17.3°, corresponding to 8% and 57% improvement compared with WSM and W/O devices, respectively. Therefore, it is certainly preferred to obtain low lateral divergences by the deeply etched microstructure.

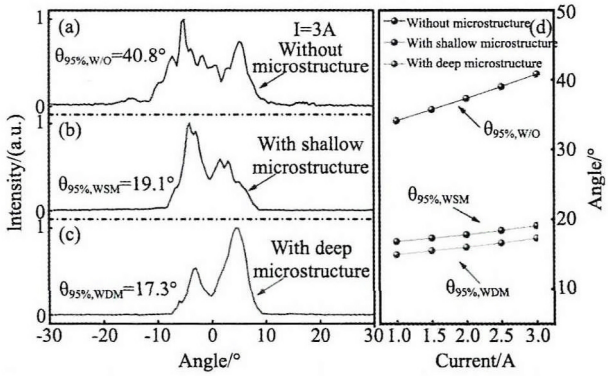

Fig. 4 Left panel: Lateral FF angles of GaSb based BA lasers at 3 A: (a) without microstructure, (b) with shallow microstructure, and (c) with deep microstructure. Right panel (d) : Measured 95% power content lateral FF angles at different currents

图4 左图: 电流为 3 A 时测试的三种类型激光器的远场特性 (a) 无结构类型,(b) 引入浅微结构类型,(c) 引入深微结构类型. 右图(d) : 测试的 95% 功率远场发散角随电流的变化

3 Conclusion

In conclusion, we have demonstrated an effective approach to improve the lateral divergence angle and emission power of 2 μm GaSb based BA lasers using a

(下转第 288 页)

[7]. *IEEE Signal Processing Magazine*, 2008, **25**(2): 21-30.
[8] Hwang B M, Sang H L, Lim W T, *et al*. A fast spatial-domain terahertz imaging using block-based compressed sensing [J]. *Journal of Infrared, Millimeter, and Terahertz Waves*, 2011, **32**(11): 1328-1336.
[9] Yi git E. Compressed sensing for millimeter-wave ground based SAR/ISAR imaging [J]. *Journal of Infrared, Millimeter, and Terahertz Waves*, 2014, **35**(11): 932-948.
[10] Herman M A, Strohmer T. High-resolution radar via Compressed sensing [J]. *IEEE Transactions on Signal Processing*, 2009, **57**(6): 2275-2284.
[11] Haupt J, Bajwa W U, Raz G, *et al*. Toeplitz compressed sensing matrices with applications to sparse channel estimation [J]. *IEEE Transactions on Information Theory*, 2010, **56**(11): 5862-5875.
[12] Abolbashari M, Farahi F. High-resolution hyperspectral single-pixel imaging system based on compressive sensing [J]. *Optical Engineering*, 2012, **51**(7): 397-407.
[13] Xiong H, Chen M, Lin Y, *et al*. Analysis of infrared images based on grey system and neural network [J]. *Kybernetes*, 2010, **39**(8): 1366-1375.
[14] Duarte M F, Davenport M A, Takbar D, *et al*. Single-pixel imaging via compressive sampling [J]. *IEEE Signal Processing Magazine*, 2008, **25**(2): 83-91.
[15] Uzeler H, Cakir S, Aytaç T. Image reconstruction for single detector rosette scanning systems based on compressive sensing theory [J]. *Optical Engineering*, 2016, **55**(2): 023108-023108.
[16] Jahng S G, Hong H K, Han S H, *et al*. Dynamic simulation of the rosette scanning infrared seeker and an infrared counter-countermeasure using the moment technique [J]. *Optical Engineering*, 1999, **38**(5): 921-928.
[17] Dai W, Milenkovic O. Subspace pursuit for compressive sensing signal reconstruction [J]. *IEEE Transactions on Information Theory*, 2009, **55**(5): 2230-2249.
[18] Lu W, Li W, Kpalma K, *et al*. Compressed sensing performance of random bernoulli matrices with high compression ratio [J]. *IEEE Signal Processing Letters*, 2015, **22**(8): 1074-1078.
[19] Tropp J A, Gilbert A C. Signal recovery from random measurements via orthogonal matching pursuit [J]. *IEEE Transactions on Information Theory*, 2007, **53**(12): 4655-4666.
[20] Needell D, Tropp J A. CoSaMP: iterative signal recovery from incomplete and inaccurate samples [J]. *Applied & Computational Harmonic Analysis*, 2008, **26**(3): 301-321.

(上接第282页)

simple microstructure. The laser devices with exceeding 1 W output power were realized. It was found that the deep microstructure could reduce the lateral-mode number more effectively. About 57% and 8% improvement in lateral FF angle were achieved with decreased peak-number and increased power from deeply etched microstructure compared with the devices without and with shallow microstructure. We believe that these results will contribute to the development of high-power low-divergence GaSb based BA diode lasers.

References

[1] Gaimard Q, Triki M, Nguyen-Ba T, *et al*. Distributed feedback GaSb based laser diodes with buried grating: a new field of single frequency sources from 2 to 3 μm for gas sensing applications [J]. *Opt. Express*, 2015, **23**: 19118-19128.
[2] Geerlings E, Rattunde M, Schmitz J, *et al*. Widely tunable GaSb-based external cavity diode laser emitting around 2.3μm [J]. *IEEE Photon. Technol. Lett.*, 2006, **18**: 1913-1915.
[3] Karsten S, Samir L, Philpp K, *et al*. 2μm laser sources and their possible applications [C/OL]. *Frontiers in Guided Wave Optics and Optoelectronics* (*Germany*: *LISA laser products OHG*). 2010(2010-02-1). http://www.intechopen.com.
[4] Belenky G, Shterengas L, Kim J G, *et al*. GaSb-based lasers for spectral region 2-4μm: challenges and limitations [J]. *Proc. SPIE*, 2005, **5732**: 169-174.
[5] Rouillard Y, Genty F, Perona A, *et al*. Edge and vertical surface emitting lasers around 2.0 ~ 2.5μm and their applications [J]. *Philos. Trans. A*, 2001, **359**: 581-597.
[6] Compeán-Jasso V H, Anda-Salazar F, de Sánchez-Niño F, *et al*. High and abrupt breakdown voltage $In_{0.15}Ga_{0.85}As_{0.14}Sb_{0.86}$/GaSb junctions grown by LPE [J]. *Infrared Phys. Technol.*, 2016, **79**: 32-35.
[7] Muller M, Rattunde M, Kaufel G. *et al*. Short-pulse high-power operation of GaSb-based diode lasers [J]. *IEEE Photon. Technol. Lett.*, 2009, **21**: 1770-1772.
[8] Gassenq A. Taliercio, T. Cerutti L, *et al*. Mid-IR lasing from highly tensile-strained, type II, GaInAs/GaSb quantum wells [J]. *Electron. Lett.*, 2009, **45**: 1320-1321.
[9] Rattunde M, Schmitz J, Kaufel G, *et al*. GaSb-based 2.X μm quantum-well diode lasers with low beam divergence and high output power [J]. *Appl. Phys. Lett.*, 2006, **88**: 08115.
[10] Wolff S, Rodionov A, Sherstobitov V E, *et al*. Fourier-optical transverse mode selection in external-cavity broad-area lasers: experimental and numerical results [J]. *IEEE Journal of Quantum Electronics*, 2003, **39**(3): 448-458.
[11] Lichtner M, Tronciu V Z, Vladimirov A G, Theoretical investigation of striped and non-striped broad area lasers with off-axis feedback [J]. *IEEE J. Quantum Electron.*, 2012, **48**: 353-360.
[12] Swint R B, Yeoh T S, Elarde V C, *et al*. Curved waveguides for spatial mode filters in semiconductor lasers [J]. *Photon. Technol. Lett.*, 2004, **16**: 12-14.
[13] Wenzel H, Crump P, Fricke J, *et al*. Suppression of higher-order lateral modes in broad-area diode lasers by resonant anti-guiding [J]. *IEEE J. Quantum Electron*, 2013, **49**: 1102-1108.
[14] Wenzel H, Bugge E, Dallmer M, *et al*. Fundamental-lateral mode stabilized high-power ridge-waveguide lasers with a low beam divergence [J]. *IEEE Photon. Technol. Lett.*, 2008, **20**: 214-216.
[15] Choi H K, Walpole J N, Turner G W, *et al*. GaInAsSb-AlGaAsSb tapered lasers emitting at 2.05 μm with 0.6 W diffraction-limited power [J]. *IEEE Photon. Technol. Lett.*, 1998, **10**(7): 938-940.
[16] Forouhar S, Briggs R M, Frez C, *et al*. High-power laterally coupled distributed-feedback GaSb-based diode lasers at 2μm wavelength [J]. *Appl. Phys. Lett.*, 2012, **100**: 031107.
[17] Rong J, Xing E, Zhang Y, *et al*. Low lateral divergence 2 μm InGaSb/ AlGaAsSb broad-area quantum well lasers [J]. *Optics Express*, 2016, **24**(7): 7246.
[18] Kelemen M T, Weber J, Mikulla M, *et al*. High-power high-brightness tapered diode lasers and amplifiers [J]. *Proc. SPIE*, 2005, **5723**: 198-208.
[19] Hecht J. Bringing high brightness to high-power laser diodes [J]. Laser Focus World, 2011, **47**(11): 43-46.
[20] Crump P, Leisher P, Matson T, *et al*. Control of optical mode distribution through etched microstructures for improved broad area laser performance [J]. *Appl. Phys. Lett.*, 2008, **92**: 131113.
[21] Jonathan A F, Mikhail A B. Federico C. Wide-ridge metal-metal terahertz quantum cascade lasers with high-order lateral mode suppression [J]. *Appl. Phys. Lett.*, 2008, **92**: 031106.
[22] Wang L, Tong C. Tian S, *et al*. High-Power Ultralow Divergence Edge-Emitting Diode Laser With Circular Beam [J]. *IEEE J. Sel. Top. Quantum Electron.* 2015, **21**(6): 1501609.
[23] Crump P, Pietrzak A, Bugge F, *et al*. 975 nm high power diode lasers with high efficiency and narrow vertical far field enabled by low index quantum barriers [J]. *Appl. Phys. Lett.*, 2010, **96**(13): 131110.